PROGRESS IN SIMULATIONS OF TURBULENT BOUNDARY LAYERS

Philipp Schlatter, Ramis Örlü, Qiang Li, Geert Brethouwer,
Arne V. Johansson, P. Henrik Alfredsson, Dan S. Henningson
Linné FLOW Centre and Swedish e-Science Research Centre (SeRC)
KTH Mechanics, SE-100 44 Stockholm, Sweden
pschlatt@mech.kth.se

ABSTRACT

Recent efforts in the simulation of turbulent boundary layers using direct and large-eddy simulations are described. The focus is naturally on a series of simulations performed at KTH Stockholm. These results have been used to examine various aspects of the boundary layer; starting from estimates of the extent of the transitional region, the detailed comparison to wind-tunnel experiments, the effect of ambient free-stream turbulence on the boundary layer and to quantifications of the spectral composition of the turbulent signal. Furthermore, selected aspects of boundary layers with coupled scalar (*e.g.* heat) transport are summarised, including profiles of the turbulent Prandtl number Pr_t.

INTRODUCTION

The study of turbulence developing close to solid walls, usually referred to as *wall turbulence* is certainly one of the most important aspects of turbulence. For instance, a large fraction of the frictional drag of moving streamlined bodies immersed in a fluid stems from the intricate vortical fluid motion close to the wall. A better understanding and consequently the possibility to affect wall turbulence in favourable ways (*flow control* to reduce drag) has important consequences for air and water-bound transportation.

The concept of the boundary layer was introduced by Ludwig Prandtl in 1904. He predicted that the influence of viscosity in a flow is mainly contained in a thin region close to the wall. During the last 100 years, significant progress has been made to disentangle the various open questions relating to the appearance of a turbulent boundary layer, but fundamental issues still remain unclear. The debate regarding the correct description of the mean velocity profile and the corresponding value of the von Kármán constant κ, the scaling of the velocity fluctuations as the Reynolds number is increased, but also various conflicting views regarding coherent vortical structures in the layer are some of the most prominent topics. An extended discussion of additional aspects is given in the recent review by Marusic *et al.* (2010).

Naturally, most studies of turbulent boundary layers were and still are performed using experimental techniques. Valuable data has been recorded in various wind-tunnel, channel and pipe facilities around the world. There are a number of research directions from an experimental point of view. Probably the most important aspect is the increase of the Reynolds-number range to be covered with accurate and reliable measurements; examples include atmospheric measurements, the Princeton superpipe and the on-going efforts around the CICLoPE project near Bologna (Talamelli *et al.*, 2009; Smits *et al.*, 2011). On the other hand, the available measurement and postprocessing techniques are improving rapidly as well. Two-dimensional and three-dimensional visualisations of wall turbulence using techniques such as particle image velocitymetry (PIV) allowed insight into the vortical composition of these flows, see *e.g.* Adrian (2007). Also, traditional measurement techniques are constantly improved, as evidenced by a number of recent studies dealing with the effect and potential correction of spatial resolution issues of hot wires (Hutchins *et al.*, 2009; Örlü & Alfredsson, 2010), and the determination of the wall position (Örlü *et al.*, 2010).

An alternative to laboratory experiments of wall flows was found in direct numerical simulations (DNS, see Kim *et al.*, 1987). Periodic turbulent channels have been the foremost flow case to be studied via numerical simulations, mainly due to the unambiguous definition of boundary conditions and the Cartesian (numerics-friendly) geometry; high Reynolds numbers in large domains have been achieved in this case (Hoyas & Jiménez, 2006). Periodic pipe flow, popular in experiments, has only recently become the subject of large-scale DNS (see *e.g.* Wu & Moin, 2008), however a number of new high-Reynolds-number simulations being underway. Turbulent boundary layers in a periodic framework, have also been avidly studied, going back to the DNS by Spalart (1988).

Spatially developing flows pose more challenges, both experimentally and numerically, as the streamwise homogeneity is lost. A typical developing boundary layer is shown in Fig. 1; it is clear that such setups require large domains for an accurate description of the physics. Proper inflow conditions and turbulence generation need to be imposed, and a sufficiently long development region necessarily needs to precede the measurement region. One of the first spatially developing turbulent boundary layer was simulationed by Skote (2001), reaching a Reynolds number $Re_\theta = 700$ based on the momentum thickness θ and the free-stream velocity U_∞. During the last years, owing to the advances in high-performance computing, new simulations in large domains have been pre-

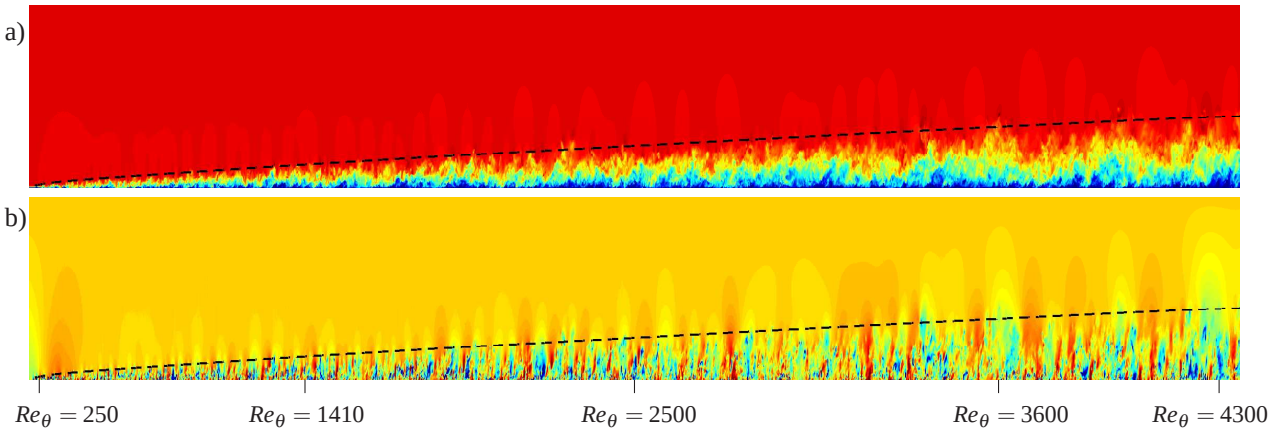

Figure 1. Instantaneous side view showing colour contours of the a) streamwise velocity and b) pressure. The domain shown corresponds to the streamwise extent of the present DNS, reaching up to approximately $Re_\theta = 4400$ (exluding the fringe region at the outflow); the full wall-normal extent of the domain is shown. – – – –99%-boundary layer thickness. The representation of the box is stretched by a factor of four in the wall-normal direction.

sented, see *e.g.* Simens *et al.* (2009) and Schlatter *et al.* (2009) reaching up to $Re_\theta \approx 2500$, and Schlatter & Örlü (2010*b*) exceeding $Re_\theta = 4000$.

The present article summarises some of the results that have been obtained using numerical simulations of turbulent boundary layers, mainly at KTH Stockholm (Sweden). In particular, the numerical method is introduced together with the spatial simulation setup. Then, a detailed comparison between DNS and experiments is presented. Further, the large outer boundary-layer structure is discussed with the help of spectra. Furthermore, additional complicating aspects such as free-stream turbulence and passive scalars are discussed last.

SIMULATION SETUP

In this section, the discretisation method of the governing equations is introduced, followed by a discussion of the spatial development leading to the fully developed turbulent state.

Numerical method

All simulations included here have been performed using our in-house spectral simulation code SIMSON (Chevalier *et al.*, 2007). The discretisation is based on a Fourier decomposition in the wall-parallel (streamwise and spanwise) directions; coupled with Chebyshev polynomials in the wall-normal direction. The pressure is eliminated by means of a velocity-vorticity formulation of the governing incompressible Navier–Stokes equations. Dealiasing of the Fourier modes is employed using the 3/2-rule, and the time integration employs a standard low-storage Runge–Kutta/Crank–Nicolson scheme. As some of the presented simulations are relatively large, considerable care has been taken in parallelising the code for use on modern supercomputers (Li *et al.*, 2008); for the largest DNS, which was running on a total of 4096 cores on the "Ekman" cluster at KTH, approximately 35% of the computational time was spent in communication between the processors. This value is very reasonable given the global character of the spatial discretisation, necessitating a global transpose operation in each step. All simulations are performed in the spatial framework, meaning that a laminar boundary layer is imposed at the inflow which is subsequently tripped to turbulence, and exhibits substantial growth as the flow is developing in the streamwise direction, see Fig. 1. In order to combine the spatial development with the requirement of periodic boundary conditions due to the Fourier discretisation, a so-called *fringe region* is added at the downstream end of the physical domain. In this region, the outflowing fluid is forced via a volume force to the laminar inflow Blasius profile (Bertolotti *et al.*, 1992; Chevalier *et al.*, 2007). Since simulations at high Reynolds numbers quickly get very expensive in terms of grid resolution and thus computer time, some of the calculations were performed using an active subgrid-scale (SGS) model, which allowed for a reduction of the numerical resolution. For these large-eddy simulations (LES) a simple but effective formulation was used, the ADM-RT model (Schlatter *et al.*, 2004), which adds additional dissipation at the small resolved scales by means of a relaxation term (RT). Compared to the fully-resolved DNS, the resolution could be reduced by about a factor of two in each direction without compromising the predictive character of the simulation results (Schlatter *et al.*, 2010*b*).

The main simulation of a turbulent boundary layer within this project was obtained in a domain spanning $Re_\theta = 180 - 4300$ and reported in Schlatter & Örlü (2010*a*). The size was chosen about three times wider and higher than the maximum δ_{99}; as Fig. 1b) shows, the free-stream is affected by comparably strong, vertically oriented pressure oscillations reaching far outside the boundary layer and have to be resolved for accurate results. A total of $8192 \times 513 \times 768$ spectral modes are employed, yielding a resolution in physical space of $\Delta x^+ \approx 9$ and $\Delta z^+ \approx 4$; $(\cdot)^+$ indicates classical viscous scaling. This resolution is comparable to high-Re channel-flow simulations such as *e.g.* Hoyas & Jiménez (2006), and slightly higher than our previous DNS (Schlatter *et al.*, 2009).

Turbulence generation

In a simulation setup based on in- and outflow conditions, turbulence needs to be continuously generated inside

the computational domain. In experiments, the natural way to achieve a turbulent boundary layer is to introduce disturbances by tripping devices (wires, roughness, *etc.*) close to the plate leading edge.

In simulations, similar measures have to be taken. The most frequently used option is the so-called *recycling method*, originally proposed by Lund *et al.* (1998) and employed among others by *e.g.* Simens *et al.* (2009). Although effective, we have chosen a different approach for the present simulations. Our inflow is located at $Re_\theta = 180$ with a laminar Blasius velocity profile. Slightly more downstream, a random volume force is implemented, which acts similar as a trip wire, in order to initiate (resolved) laminar-turbulent transition at a fixed location and reach turbulence as soon as possible without affecting the natural development (Schlatter *et al.*, 2010*c*). The immediate question is of course to what extent the precise details of the inflow and tripping are affecting the flow development, and how far downstream (*i.e.* at which Reynolds number) a fully developed turbulent boundary-layer flow can be expected. This is in particular important when comparing data to other methods (*e.g.* the recycling or experiments).

To study the dependence of the boundary layer on initial conditions, a series of DNS with varying tripping parameters has been performed. Fig. 2a) shows the friction coefficient c_f as a function of Re_θ; it can clearly be seen that for all DNS the inflow is laminar (*i.e.* $c_{f,\mathrm{lam}} = 0.441 Re_\theta^{-1}$). Depending on tripping, laminar-turbulent transition occurs at different Re_θ, but the curves quickly settle on a common c_f distribution, indicating a rather quick adaptation of the near-wall turbulence. It further turns out that the turbulent value $c_{f,\mathrm{turb}}$ can be well described using the simple relation $c_f = 0.024 Re_\theta^{-0.25}$ (Smits *et al.*, 1983). Note also the typical overshoots of c_f as a result of transition. On the other hand, as shown in Fig. 2b), the outer-layer convergence, illustrated by contours of u_{rms}, requires much longer development length than near the wall. It is this effect which might explain some of the differences observed while comparing DNS data of different origin (Schlatter & Örlü, 2010*a*). It remains an open question what conditions to apply to determine whether a boundary layer has reached a "fully-turbulent" state, but it is clear that the skin friction close to the wall is not sufficient. For the present data, if transition was initiated at low enough $Re_\theta < 300$, all data agree well for both inner and outer layer for $Re_\theta > 2000$, which is also the value for which reliable wind-tunnel results have been reported (Örlü, 2009). For our base-line simulation, based on the comparison given in Fig. 2, we conjecture that $Re_\theta \approx 500$ is the lowest reliable streamwise position (Schlatter & Örlü, 2011).

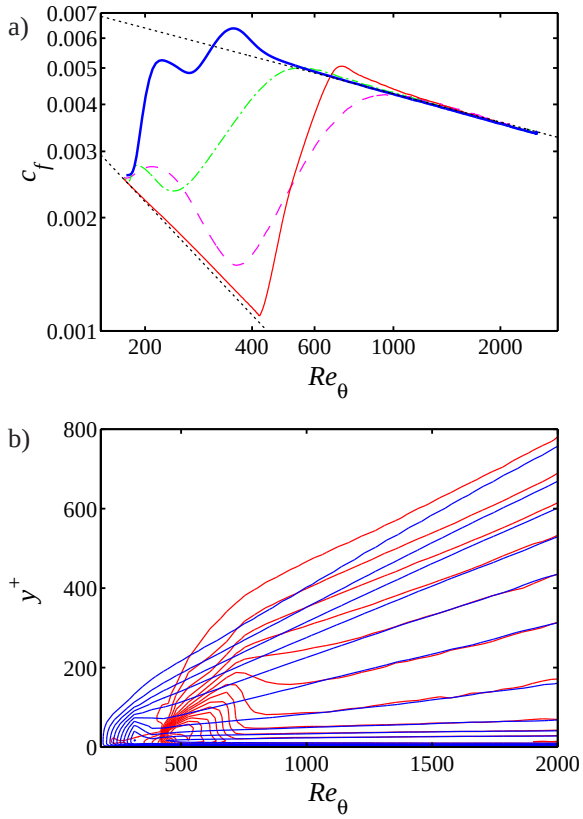

Figure 2. a) Skin-friction coefficient c_f for various trippings: ——— "baseline" case, –·–· lower amplitude and – – – – lower frequency trippings, ——— "classical" transition via exponential growth of TS waves. ····· Correlations for laminar ($c_f = 0.441 Re_\theta^{-1}$) and turbulent ($c_f = 0.024 Re_\theta^{-0.25}$) flow. b) Contours of u^+_{rms} (spacing 0.25) for baseline case (blue) and TS-wave case (red).

DNS AND EXPERIMENT

The importance of inflow and upstream conditions in the simulation of spatially developing flows has been emphasised in the previous section, and as illustrated through the various tripping mechanisms and transition scenarios a common trend can be achieved at $Re_\theta \approx 2000$ (Schlatter & Örlü, 2011). These observations go along with experimental findings (Erm & Joubert, 1991) and explain to a large extend the documented differences in basic integral quantities between available DNS from zero pressure-gradient (ZPG) turbulent boundary layer flows (Schlatter & Örlü, 2010*a*). While inflow and upstream conditions can precisely be set in simulations, these are often not fully assessed and/or documented in experiments (Chauhan *et al.*, 2009). This consequently pushes the lower limit for any serious cross-validation of experiments and simulations to the mentioned Re_θ value of 2000, in order to ensure that the differences are not mere reminiscences of different inflow and upstream conditions. Furthermore, detailed knowledge about how quantities have been computed are essential for meaningful and insightful comparisons (Chauhan *et al.*, 2009; Schlatter & Örlü, 2010*a*).

Based on these considerations experimental investigations by means of hot-wire and oil-film interferometry measurements have accompanied the numerical efforts in close collaboration, and first results have shown considerable agreement in integral quantities as well as mean and rms profiles (Schlatter *et al.*, 2009). Recalling the differences in compiled experimental (Fernholz & Finley, 1996; Chauhan *et al.*, 2009) and numerical data (Schlatter & Örlü, 2010*a*) sets, the found agreement in *e.g.* the skin-friction coefficient c_f is exceptional as apparent from Fig. 3. Similarly, the shape factor shows perfect agreement and, albeit not shown here, can be anticipated from the overlapping of both data sets throughout the boundary layer as apparent from Fig. 4 depicting the inner-scaled

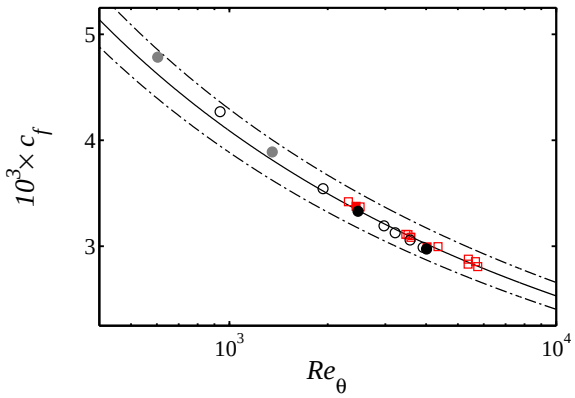

Figure 3. Skin-friction coefficient c_f as function of Reynolds number Re_θ. ——— correlations given by Chauhan *et al.* (2009) with —·— ±5% tolerance for c_f. Present DNS (◯) and experimental data (□); the streamwise positions indicated through filled symbols are further discussed in Fig. 4.

mean and rms profiles. Inspection of the velocity gradient, in form of the indicator function Ξ emphasises the excellent agreement, but also underlines that the present DNS, albeit the highest reported in terms of Re_θ, is merely at the verge from where on the indicator function reaches a plateau, *i.e.* the von Kármán constant can indeed be considered constant (Monkewitz *et al.*, 2007).

A closer look at the near-wall peak in the rms profiles, on the other hand, reveals marginal differences: while a clear increase in the near-wall peak with *Re* is present in case of the DNS, the experimental data depict the opposite trend. This can, however, completely be explained by insufficient spatial resolution of the hot-wire probe (Örlü & Alfredsson, 2010). DNS can be averaged in the spanwise direction in order to examine the effect of the length of the measurement sensor and thereby resemble the experimental data as demonstrated. Available DNS data has very recently been utilised to simulate the effect of spatial averaging effects of hot-wire probes (see *e.g.* Örlü *et al.*, 2010) as also demonstrated in the inset of Fig. 4. Besides heuristic models that need to be calibrated against available data, data-driven schemes utilising two measurements with different wire length can be exploited to obtain a very good estimate of the rms profile as apparent from Fig. 5, but also obtain the difficult to measure spanwise Taylor microscale (Segalini *et al.*, 2011).

The aforementioned comparison between DNS and experimental data has pointed out that DNS resembles the experimental data in integral, mean and higher order quantities when spatial resolution effects are taken into account to a high degree as demonstrated through the contour map of the probability density functions (PDF) depicted in Fig. 6 (Örlü & Schlatter, 2011*b*). The advantage of having access to minutiae details of the DNS and experimental data, and a consistent re-evaluation of integral and statistical quantities highlights every apparent difference between the data sets as something worth to investigate. Such an apparent difference appears *e.g.* in the viscous sublayer, a region difficult to explore experimentally. Hot-wire measurements are known to be affected by near-wall effects in the viscous sublayer which lead the measured mean velocity to appear higher than it actually is. The

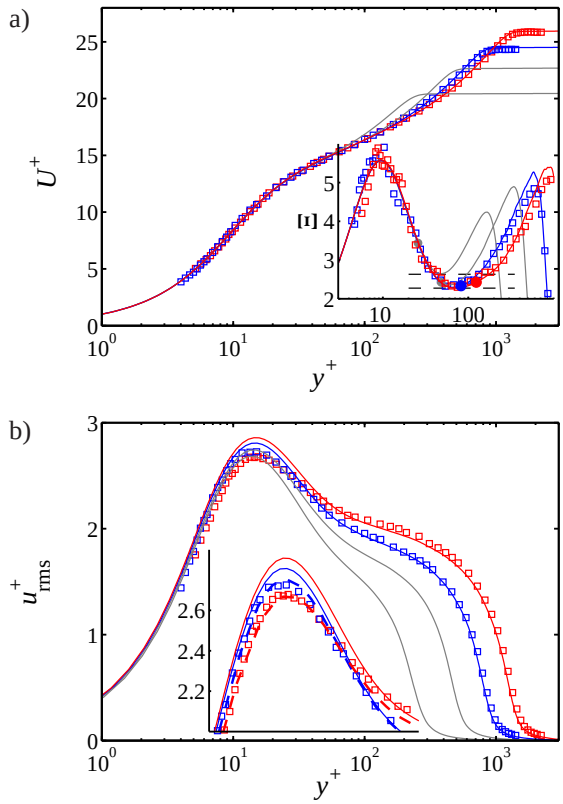

Figure 4. a) Inner-scaled mean streamwise velocity profile and indicator function. Numerical (—) and experimental data (□) for Re_θ highlighted in Fig. 3, *i.e.* Re_θ = 670, 1410, 2500, 4000. The upper limit of the overlap region, defined as $y^+ = 0.1\delta^+_{99}$, (•) as well as $\kappa = 0.38$ and 0.44 (– – –) is given as well in the indicator plot (inset). b) Inner-scaled turbulence intensity profile with inset enlarging the near-wall peak region. Dashed lines represents spanwise averaged DNS data in order to match viscous-scaled hot-wire length (i.e. $\Delta z^+ \approx L^+$).

detailed comparison of the PDF in Fig. 6 shows that the region in which the hot-wire experiences additional heat losses to the wall is not only a function of the wall distance, but depends on the instantaneous velocity as well. Since the high velocity fluctuations within the viscous sublayer follow the DNS (parallel contours) this part of the PDF can actually be exploited to obtain an accurate estimate of the wall position and friction velocity as demonstrated in Alfredsson *et al.* (2011*a*).

To conclude this section, Fig. 7 shows the rms of the wall shear stress and wall pressure; both of these quantities have been used as diagnostic quantities for turbulent wall flows. As predicted by Alfredsson *et al.* (1988) and confirmed recently by Örlü & Schlatter (2011*a*), a value for $\tau^+_{w,\rm rms}$ of around 0.4 with a slight increase with *Re* is found. Schlatter & Örlü (2010*a*) proposed a relation $\tau^+_{w,\rm rms} = 0.298 + 0.018 \ln Re_\tau$ which agrees well with DNS data. Similarly, for the wall pressure fluctuations $p^+_{w,\rm rms}$, good agreement with the experimental correlation by Farabee & Casarella (1991) was demonstrated by Schlatter *et al.* (2010*b*). For both quantities, the recent simulation by Wu & Moin (2010) shows discrepancies

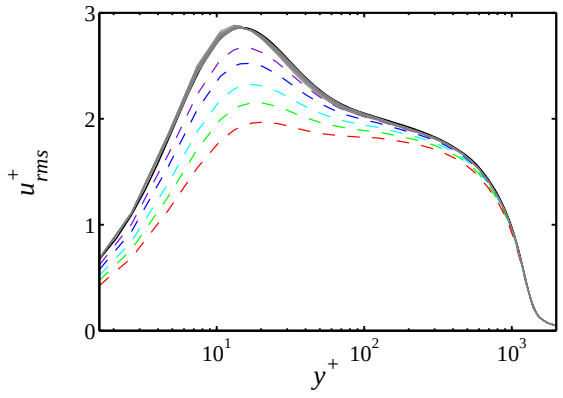

Figure 5. Inner-scaled rms profiles for $Re_\theta = 4000$. Profiles with Δz^+ (equivalent to L^+) of 22, 33, 49, 65 and 87, are simulated by spanwise filtering of the DNS and are depicted through dashed lines, while reconstructed profiles through the method proposed by Segalini *et al.* (2011) are given through solid lines.

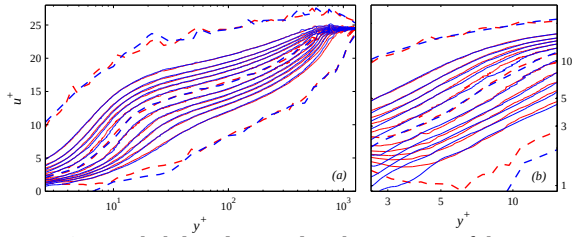

Figure 6. Probability density distribution map of the streamwise velocity at $Re_\theta = 2500$ for experimental (red) and DNS (blue) data. Solid contours indicate 10, 30, 50, 70, and 90 % of the local peak PDF value (centered dashed line), whereas the outer dashed lines include all sampled velocity signals, *i.e.* the maximum values of the pdf.

to most other data; the origin of this behaviour is unknown.

STRUCTURE OF THE BOUNDARY LAYER

In this section, several aspects of a turbulent boundary layer relating to the structure of the turbulence are considered. In particular, the appearance of scales of diverse size are discussed and its influence on the wall shear stress is shown together with a few two-dimensional spectral cuts through the boundary layer.

Large and small scales

Probably the most ubiquitous feature of wall turbulence is the appearance of streamwise elongated regions of alternating high and low speed. These so-called turbulent streaks are located in the buffer layer (*i.e.* at around $y^+ \approx 12$), and intimately relate to the near-wall regeneration cycle of wall turbulence. Whereas these structures are dominating the whole turbulent flow field at low to moderate Reynolds numbers, a second spectral peak is slowly appearing for higher Reynolds numbers, located further away from the wall, $y/\delta_{99} \approx 0.1$. Whether or not this peak is becoming most dominant for large

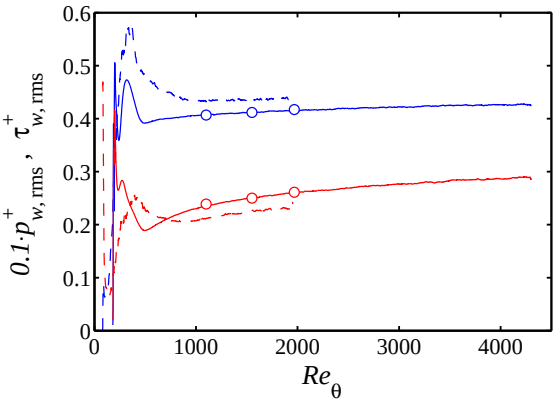

Figure 7. Wall pressure fluctuations $p^+_{w,\mathrm{rms}}$ (red) and wall shear stress fluctuations $\tau^+_{w,\mathrm{rms}}$ (blue). ——— Present DNS, ◯ DNS by Simens *et al.* (2009), – – – – DNS by Wu & Moin (2010).

Re is part of ongoing research (Alfredsson *et al.*, 2011*b*). In Fig. 8 a visualisation of a short part of the DNS data at $Re_\theta = 4300$ is shown (Schlatter *et al.*, 2010*c*); giving an impression of the range of scales present at such Reynolds numbers. Taking the same data, and looking along the streamwise coordinate as in Fig. 9 a large-scale corrugation of the boundary layer edge is apparent; its spanwise wavelength is clearly related to the thickness of the layer. Furthermore, from this figure it can be inferred that the state of turbulence is dependent on whether it lies directly below a large-scale low-speed or high-speed region. This modulation of the near-wall scale by the outer layer has been discussed and quantified in *e.g.* Mathis *et al.* (2009) and Schlatter & Örlü (2010*b*).

Recent DNS results by Wu & Moin (2010) noted that – at least at low *Re* close to transition – the classical *hairpin vortex* as suggested by Theodorsen appears to be a dominant vortical structure in the turbulent flow. In our data, close to where transition is initiated ($Re_\theta < 800$), indeed a "forest of hairpins" could be observed. However, these highly organised structures quickly loose their coherency as the Reynolds number is increased, and at *e.g* $Re_\theta = 4300$ (Fig. 8), the flow is dominated by a more or less random conglomerate of vortex tubes without clear large or small-scale hairpin vortices. Moreover, conditional averaging was used close to the wall to identify the most dominant instability mechanism, which turns out to be of sinuous type in agreement with channels (Jeong *et al.*, 1997). An animated view of the turbulent boundary layer data, and a discussion of the flow structures appearing close to transition as opposed to the fully turbulence state is provided in a video (Schlatter *et al.*, 2010*a*).

Wall shear stress

The turbulence right at the wall, namely the instantaneous wall shear stress τ_w, is an important quantity as it directly measures the amount of frictional force exerted on the wall. On the other hand, τ_w is also modified by the turbulence conditions further away from the wall, *i.e.* the (outer) Reynolds number as discussed above. In a recent study of the shear-stress fluctuations $\tau^+_{w,\mathrm{rms}}$ (Örlü & Schlatter, 2011*a*), prompted by the DNS of Wu & Moin (2010), we examined

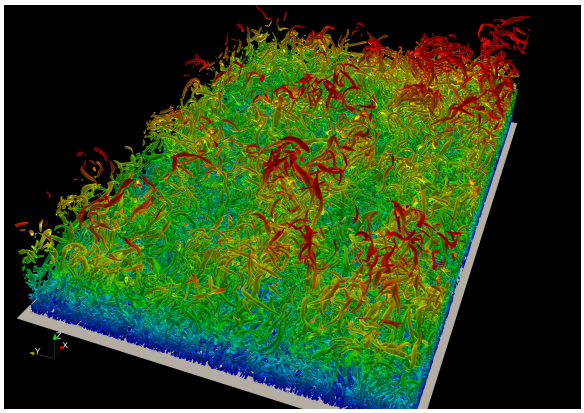

Figure 8. Visualisation of the structures in a turbulent boundary layer by means of isocontours of negative λ_2 (Jeong & Hussain, 1995); the colour code represents the wall distance. The middle of the visualised domain is located at about $Re_\theta = 4300$.

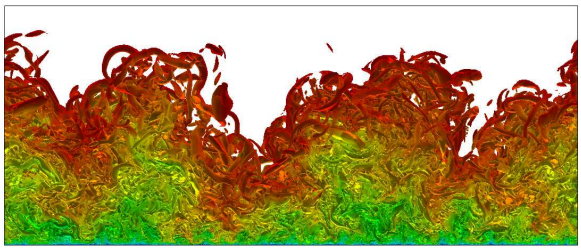

Figure 9. Front view of a vertical slice through the boundary layer at $Re_\theta = 4300$ showing isocontours of negative λ_2; same data as Fig. 8, real aspect ratio (height is about $1.2\delta_{99}$). The colour coding indicates streamwise velocity, ranging from zero (blue) to one (red). The large-scale corrugation of the boundary-layer edge plus the induced modulation of the near-wall structures is clearly visible.

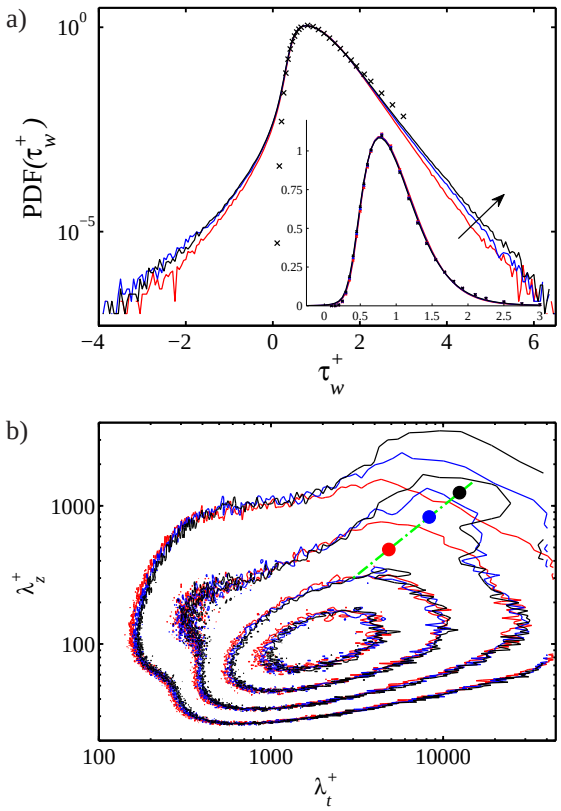

Figure 10. a) Probability density function (PDF) of τ_w^+ for $Re_\theta = 1100$, 2500 and 4000. Inset depicts the same three PDFs with a linear ordinate together with a lognormal PDF ($\times$) fitted to the three DNS data sets. Arrow indicates increasing Re_θ. b) Two-dimensional premultiplied spectra of τ_w^+ for $Re_\theta = 1100$, 2500 and 4000 as function of spanwise wavelength and temporal period. Contour levels are chosen as 0.15, 0.4, 1.0, and 2.0, while the dashed line indicates $\lambda_t^+ = 10\lambda_z^+$, and the filled circles $\lambda_z^+ = Re_\tau$.

the time-histories of the boundary-layer DNS data. In Fig. 10, PDFs and two-dimensional premultiplied spectra are shown. It can be seen that classical viscous scaling provides a good collapse of the PDF, except for a widening of the tails with higher Re_θ. Interesting in that respect is that a region with clearly negative shear stress (instantaneous flow reversal) exists. The occurrence is seldom ($< 0.1\%$) but not negligible.

The premultiplied spectrum of τ_w in Fig. 10b) gives an explanation of why the total shear-stress fluctuation slowly increases with Reynolds number (see previous discussion). Inner scaling provides an excellent collapse for most of the spectrum, except the upper right corner characterised by wide (large λ_z) and long-lasting (large λ_t) scales: It is exactly this region which is progressively influenced by the large-scale motion discussed in the previous section, and leaves its footprint on the wall shear stress. Similar observations have also been reported *e.g.* from channel flow (Abe *et al.*, 2004).

Spectral information

A further quantitative description of the distribution of scales throughout the boundary layer can be obtained by considering one- and two-dimensional spectra. As commonly done, premultiplied spectra are used, since this provides a convenient way to directly estimate the energy content when plotted against a logarithmic abscissa. In Fig. 11 a one-dimensional spectrum of the streamwise velocity at $Re_\theta = 4000$ is shown. Clearly, the inner peak related to the wall-layer streaks with typical spanwise size of about 120 plus units (Schlatter *et al.*, 2009) is most dominant. However, with a spanwise scale of about $0.85\delta_{99}$ a second isolated peak appears (see also the LES data in Schlatter *et al.*, 2010*b*). Since a one-dimensional spectrum only provides scale information integrated in time, it is also interesting to consider true two-dimensional spectra in a (spanwise/time), λ_z/λ_t plane, recorded at three wall-normal locations throughout the boundary layer, see Fig. 12. Closest to the wall, Fig. 12a), the turbulent streaks are obvious. Rescaling the time scale with an appropriate convection velocity of the near-wall small scales, the typical length of about 1000 plus units is recovered as expected. As for the wall shear stress, a weak outer peak is apparent in the 2D spectrum. Moving away from the wall, Figs. 12b) and c), the range of excited spanwise and temporal scales

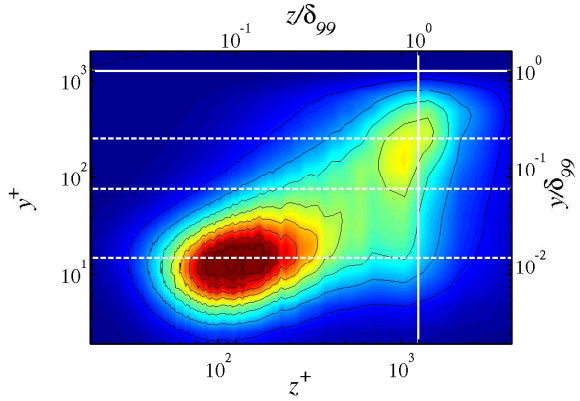

Figure 11. Premultiplied spanwise energy spectrum of the streamwise velocity at $Re_\theta = 4000$, scaled in inner units; contour lines are separated by 0.4. The solid line indicate $y^+ = \lambda_z^+ = \delta_{99}^+ = 1250$, and the dashed lines $y^+ = 15$, 75 and $y/\delta_{99} = 0.2$ (see Fig. 12).

changes, but the outer peak retains its size in terms of outer units, $\lambda_z = 0.85\delta_{99}$ and $\lambda_t = 10U_\infty/\delta_{99}$. The latter time can be converted into a length scale by assuming a (large-scale) convection velocity, giving approximately $\lambda_x = 6\delta_{99}$ which corresponds well with experimental findings (Hutchins & Marusic, 2007) and previous LES (Schlatter *et al.*, 2010*b*).

PASSIVE SCALARS

Scalar transport phenomena have been studied for a long time due to their importance for combustion, mixing and in environmental applications. However, in the literature there are only few numerical works considering passive scalar transport in flat-plate turbulent boundary-layer flows; reasons are probably very similar as mentioned in the Introduction related to a proper setup of a spatially developing boundary layer. The first data were presented by Bell & Ferziger (1993) considering three scalars: Pr being $0.1, 0.71$ and 2.0 up to a low Reynolds number of $Re_\theta = 700$. Araya (2008) performed a LES from $Re_\theta = 2000$ to $Re_\theta = 2400$ with $Pr = 0.71$. All these simulations use variations of the recycling method to generate turbulent inflow conditions. The only simulations which contain also laminar-turbulent transition as discussed above were performed by Li *et al.* (2009) up to $Re_\theta \approx 850$ (DNS), and by Wu & Moin (2010) up to $Re_\theta = 1950$ with $Pr = 1.0$. With a similar setup as the former DNS, a LES was recently performed by Li & Schlatter (2011) reaching $Re_\theta \approx 2500$, in order to provide good reference data.

One of the most important coefficients for scalar transport is the turbulent Prandtl number which is defined as the ratio of the turbulent eddy viscosity to the eddy diffusivity. Almost all turbulence models for scalar transport rely on the turbulent Prandtl number in some way, thus a large body of literature has been devoted to Pr_t, see *e.g.* the review by Kays (1994). Assuming the so-called Reynolds analogy, Pr_t is usually assumed constant and of order unity; experimentally this has been confirmed with good accuracy for $y^+ \geq 50$ with values of 0.85 in the log region and dropping to about 0.6 in the wake region. However, contradictory results are observed for $y^+ \leq 50$. Firstly, in the DNSs by Bell & Ferziger (1993); Li

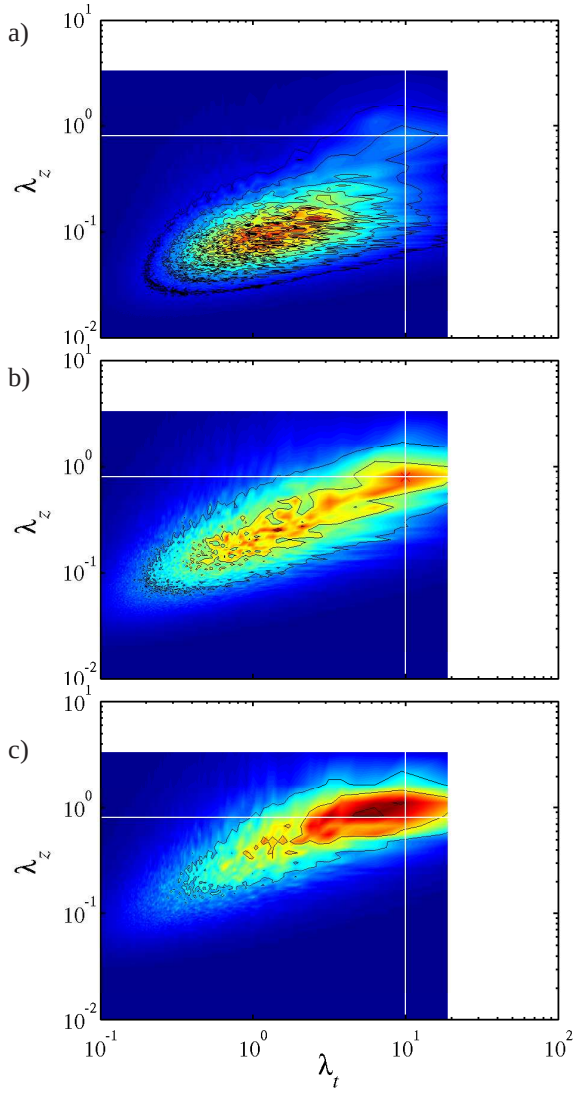

Figure 12. Two-dimensional premultiplied spectrum of the streamwise velocity fluctuations measured at $Re_\theta = 4000$ at $y^+ = 15, 75$ and $y/\delta_{99} = 0.2$. White lines indicate $\lambda_z = 0.8\delta_{99}$ and $\lambda_t = 10U_\infty/\delta_{99}$.

et al. (2009) and others, there is a mild upward "bulge" existing at $y^+ = 40 - 50$. However, none of the experimental data show such a "bulge". Secondly, starting from $y^+ = 20 - 30$, a substantial rise of the turbulent Prandtl number is observed in most experimental data, whereas simulations only show a very gentle increase starting from $y^+ = 10 - 20$, and saturate to a constant wall-limiting value below $y^+ \approx 1$. This constant wall-limiting behaviour is also consistent with near-wall asymptotics. Kays (1994) speculated that the main difference between the experimental and the DNS results is the difference in the Reynolds number. Based on our current DNS and LES data, however, it becomes clear that Re_θ does not change the near-wall behaviour significantly, see Fig. 13. The recent DNS data by Wu & Moin (2010) at $Re_\theta = 1840, Pr = 1$ is also shown in the figure for comparison: Their near-wall behaviour is clearly different from all the other simulation results; it increases monotonically towards the wall and there is

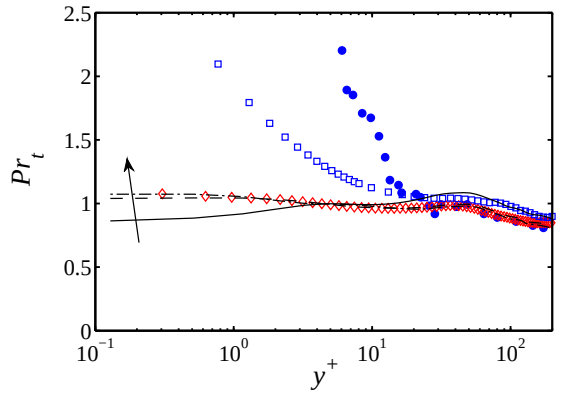

Figure 13. Turbulent Prandtl number. Simulation at $Re_\theta = 1840$ (Li & Schlatter, 2011), ——— $Pr = 0.2$, – – – – $Pr = 0.71$, —·—·— $Pr = 2.0$ (in direction of the arrow). □ Wu & Moin (2010). ◯ Blackwell *et al.* (1972), ◇ Abe *et al.* (2004) (channel at $Re_\tau = 640$).

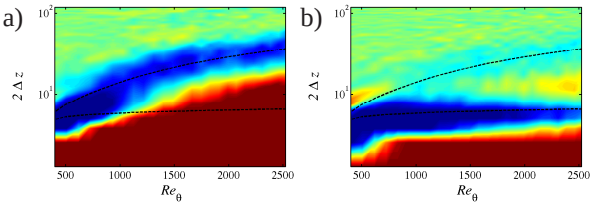

Figure 14. Spanwise two-point correlation of the wall heat flux $R_{q_w q_w}$. a) $Pr = 0.2$; b) $Pr = 2.0$. Colours range from -0.06 to 0.06, – – – – $0.85\delta_{99}$ and 120 plus units.

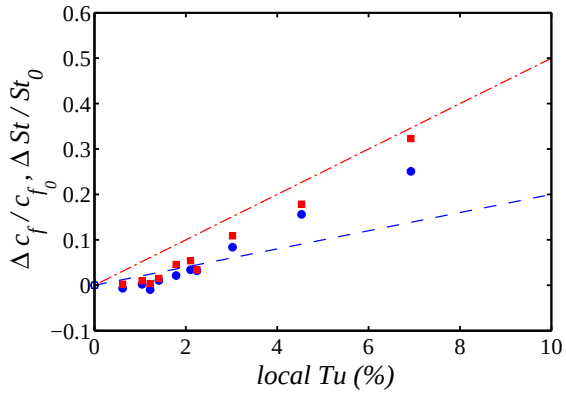

Figure 15. Relative increase of the skin-friction coefficient c_f and the Stanton number St versus the local turbulence intensity at $Re_\tau = 300$. ○ c_f, □ St; Correlation from Ref. Simonich & Bradshaw (1978): – – – – $\Delta c_f/c_{f0}$=2Tu, —·— $\Delta St/St_0$=5Tu.

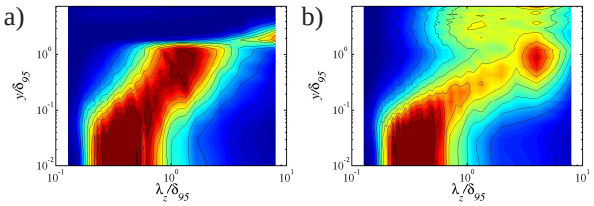

Figure 16. Premultiplied spanwise energy spectra of $\Phi_{uu}(\lambda_z)/u^2_{rms}$. a) Case without FST at $Re_\tau = 300$. b) Local $Tu = 7\%$ at $Re_\tau = 330$. The colours range from blue (0.0) to red (0.5). Contour lines are from 0 to 0.5 with spacing 0.05.

no upward "bulge" at $y^+ = 40 - 50$. It remains unclear why there is such a difference, but given the importance of Pr_t this issue is certainly important to resolve.

The effect of the (molecular) Prandtl number Pr on the scales present in the scalar field can be easily appreciated via the spanwise two-point correlation of the wall heat flux $R_{q_w q_w}$ in Fig. 14 for two cases with different Prandtl numbers, *i.e.* $Pr = 0.2$ and 2.0 (Li & Schlatter, 2011). Compared to the distribution of the wall shear stress, see Schlatter *et al.* (2009), the picture is clearly different although Pr is not far from unity. For lower Pr, Fig. 14a) the first minimum in the wall heat flux arises at $\Delta z \approx 0.85\delta_{99}$, indicating that the modulation of q_w due to the outer-layer structures is very dominant; the inner peak corresponding to the near-wall streaks is absent from the heat flux with $Pr = 0.2$. The exact opposite behaviour can be observed for high $Pr = 2.0$: The dominant spanwise scale is the inner peak ($\Delta z^+ = 120$), and only weak modulation at larger scales is visible.

FREE-STREAM TURBULENCE

A completely quiet free-stream is of course an idealisation of real cases in both engineering and nature. In particular in turbomachinery applications, high levels of ambient free-stream turbulence (FST) intensity Tu are often present. A boundary layer developing below free-stream turbulence will usually undergo rapid, so-called bypass transition, see *e.g.* Matsubara & Alfredsson (2001), before reaching a turbulent state. However, sufficiently strong FST will continue to affect the turbulent boundary layer even after transition. The pioneering works in this field were performed by Bradshaw (1974). One primary observation is that the skin friction at the wall is measurably increased due to the FST. Similarly, the Stanton number St describing the non-dimensional heat flux, is increased at an even higher rate, implying that the Reynolds analogy does not hold any longer when FST is present. Our simulation results, presented by Li *et al.* (2010) and also shown in Fig. 15, support this experimental finding; local Tu of 6% increases the skin friction by roughly 20%. Mean velocity profiles recorded with and without FST clearly show that up to the logarithmic region the flow seems to be insensitive to the FST, whereas the wake region is significantly depressed with increasing Tu. The connection to FST is given by a reduced intermittency of the outer region due to the high levels of ambient FST.

The change of the outer region due to FST is further illustrated by the premultiplied spanwise spectra, shown in Fig. 16. Without FST, two distinct spectral peaks are observable as previously discussed. Note that in Fig. 16 a scaling of the energy with $u_{\rm rms}$ has been chosen, whereas in Fig. 11 a scaling with u_τ was employed. With FST, however, the energy spectra and in particular the dominating outer peak is changed, see Fig. 16b). The most dominant peak appears now right at the boundary-layer edge, $y \approx \delta_{95}$. Meanwhile, the spanwise scale is increasing from about δ_{95} to $4\delta_{95}$; with the chosen scaling

the FST is clearly overshadowing the internal spectral composition of the boundary layer. This behaviour is similar to recent experiments by Sharp *et al.* (2009). They reported that the streamwise scale changes from $6\delta_{99}$ to $15\delta_{99}$.

CONCLUSIONS

In this review article, results obtained from simulations of spatially evolving turbulent boundary layers are summarised. In particular the spatial development of the flow poses a few important challenges which have to be addressed: Turbulence needs to be continuously fed into or generated inside the domain; the flow has to develop for a sufficiently long distance until a fully-developed state has been achieved, and large (long, wide and high) computational domains are necessary for capturing the correct physics of the flow.

During the last years, at KTH Stockholm, we have considered turbulent boundary layers using various simulation techniques. These studies culminated in a large DNS spanning the extended Reynolds-number range $Re_\theta = 180$ to 4300 in a computational box discretised with about 7.5 billion grid points. Results from this DNS have been carefully compared to experiments obtained at comparable Re_θ, and excellent agreement is obtained for both mean and fluctuating quantities. This clearly shows that, if both experiment and simulation are performed with care and parameters are matched exactly, very good agreement can be achieved.

Results are also presented pertaining to other aspects of turbulent boundary layers, such as the appearance of coherent structures in the outer layer and their influence on the wall shear stress and two-dimensional spectra. It is shown that these structures scale in outer units and are about $0.8\delta_{99}$ wide and persist for $10U_\infty/\delta_{99}$ time units; clear footprints of these structures are found starting from the wall up to the edge of the log region. However, no hairpin vortices at higher *Re* could be detected in our data.

Finally, recent simulations pertaining to scalar transport are discussed. It is shown that the turbulent Prandtl number indeed reaches a constant value close to unity at the wall, with a weak *Pr* influence. Further, the influence of free-stream turbulence on the boundary layer is summarised, and it is shown that the heat and momentum transfer is significantly increased by ambient disturbances. The outer peak of the boundary layer is completely changed under these conditions.

Data obtained from these simulations is available online on `www.mech.kth.se/~pschlatt/DATA/`.

ACKNOWLEDGEMENTS

Financial support from the Swedish Research Council (VR) is gratefully acknowledged. Computer time was provided by the Swedish National Infrastructure for Computing (SNIC) with a generous grant by the Knut and Alice Wallenberg (KAW) Foundation. The simulations were run at PDC/KTH and at NSC/Linköping University in Sweden.

The authors would also like to acknowledge NORDITA for the support in organising a research programme during April 2010 in Stockholm, Sweden. In particular, Fazle Hussain, Hiroyuki Abe, Neil Sandham, Gary Coleman, Mattias Chevalier and Yvan Maciel are acknowledge for stimulating discussions.

REFERENCES

Abe, H., Kawamura, H. & Choi, H. 2004 Very large-scale structures and their effects on the wall shear-stress fluctuations in a turbulent channel flow up to $Re_\tau = 640$. *J. Fluids Eng.* **126**, 835–843.

Adrian, R. J. 2007 Hairpin vortex organization in wall turbulence. *Phys. Fluids* **19** (041301), 1–16.

Alfredsson, P. H., Johansson, A. V., Haritonidis, J. H. & Eckelmann, H. 1988 The fluctuating wall-shear stress and the velocity field in the viscous sublayer. *Phys. Fluids* **31**, 1026–1033.

Alfredsson, P. H., Örlü, R. & Schlatter, P. 2011*a* The viscous sublayer revisited - exploiting self-similarity to determine the wall position and friction velocity. *Exp. Fluids* Online first.

Alfredsson, P. H., Segalini, A. & Örlü, R. 2011*b* A new scaling for the streamwise turbulence intensity in wall-bounded turbulent flows and what it tells us about the "outer" peak. *Phys. Fluids* **23** (041702).

Araya, G. 2008 Numerical heat transfer analysis in turbulent wall bounded flows. PhD thesis, Rensselaer Polytechnic Institute, Troy, New York, U.S.A.

Bell, D. M. & Ferziger, J. H. 1993 Turbulent boundary layer DNS with passive scalars. In *Near-Wall Turbulent Flows* (ed. R. M. C. So, C. G. Speziale & B. E. Launder), pp. 327–366. Elsevier, Amsterdam, The Netherlands.

Bertolotti, F. P., Herbert, T. & Spalart, P. R. 1992 Linear and nonlinear stability of the Blasius boundary layer. *J. Fluid Mech.* **242**, 441–474.

Blackwell, B. F., Kays, W. M. & Moffat, R. J. 1972 The turbulent boundary layer on a porous plate: *a*n experimental study of the heat transfer behavior with adverse pressure gradients. *Tech. Rep.* Report HMT-16. Thermosciences Division, Department of Mechanical Engineering, Stanford University, C.A., U.S.A.

Bradshaw, P. 1974 Effect of free-stream turbulence on turbulent shear layers. *Tech. Rep.* Aero Report 74-10. Imperial College of Science and Technology, Department of Aeronautics, London, U.K.

Chauhan, K. A., Monkewitz, P. A. & Nagib, H. M. 2009 Criteria for assessing experiments in zero pressure gradient boundary layers. *Fluid Dyn. Res.* **41** (021404).

Chevalier, M., Schlatter, P., Lundbladh, A. & Henningson, D. S. 2007 SIMSON - A Pseudo-Spectral Solver for Incompressible Boundary Layer Flows. *Tech. Rep.* TRITA-MEK 2007:07. KTH Mechanics, Stockholm, Sweden.

Erm, L. P. & Joubert, P. N. 1991 Low-Reynolds-number turbulent boundary layers. *J. Fluid Mech.* **230**, 1–44.

Farabee, T. M. & Casarella, M. J. 1991 Spectral features of wall pressure fluctuations beneath turbulent boundary layers. *Phys. Fluids* **3**, 2410–2420.

Fernholz, H. H. & Finley, P. J. 1996 The incompressible zero-pressure-gradient turbulent boundary layer: an assessment of the data. *Prog. Aerospace Sci.* **32**, 245–311.

Hoyas, S. & Jiménez, J. 2006 Scaling of the velocity fluctuations in turbulent channels up to $Re_\tau = 2003$. *Phys. Fluids* **18** (011702).

Hutchins, N. & Marusic, I. 2007 Large-scale influences in near-wall turbulence. *Phil. Trans. R. Lond. Soc. A* **365**, 647–664.

Hutchins, N., Nickels, T. B., Marusic, I. & Chong, M. S. 2009

Hot-wire spatial resolution issues in wall-bounded turbulence. *J. Fluid Mech.* **635**, 103–136.

Jeong, J. & Hussain, F. 1995 On the identification of a vortex. *J. Fluid Mech.* **285**, 69–94.

Jeong, J., Hussain, F., Schoppa, W. & Kim, J. 1997 Coherent structures near the wall in a turbulent channel flow. *J. Fluid Mech.* **332**, 185–214.

Kays, W. M. 1994 Turbulent Prandtl number - Where are we?. *ASME J. Heat Transfer* **116**, 284–295.

Kim, J., Moin, P. & Moser, R. 1987 Turbulence statistics in fully developed channel flow at low Reynolds number. *J. Fluid Mech.* **177**, 133–166.

Li, Q. & Schlatter, P. 2011 LES of a spatially developing turbulent boundary layer with passive scalar transport. Submitted.

Li, Q., Schlatter, P., Brandt, L. & Henningson, D. S. 2009 DNS of a spatially developing turbulent boundary layer with passive scalar transport. *Int. J. Heat Fluid Flow* **30**, 916–929.

Li, Q., Schlatter, P. & Henningson, D. S. 2008 Spectral simulations of wall-bounded flows on massively parallel computers. *Tech. Rep.*. KTH Mechanics, Stockholm, Sweden.

Li, Q., Schlatter, P. & Henningson, D. S. 2010 Simulations of heat transfer of a boundary layer subject to free-stream turbulence. *J. Turbulence* **11** (45).

Lund, T. S., Wu, X. & Squires, K. D. 1998 Generation of turbulent inflow data for spatially-developing boundary layer simulations. *J. Comput. Phys.* **140**, 133–158.

Marusic, I., McKeon, B. J., Monkewitz, P. A., Nagib, H. M., Smits, A. J. & Sreenivasan, K. R. 2010 Wall-bounded turbulent flows at high reynolds numbers: Recent advances and key issues. *Phys. Fluids* **22** (065103).

Mathis, R., Hutchins, N. & Marusic, I. 2009 Large-scale amplitude modulation of the small-scale structures in turbulent boundary layers. *J. Fluid Mech.* **628**, 311–337.

Matsubara, M. & Alfredsson, P. H. 2001 Disturbance growth in boundary layers subjected to free-stream turbulence. *J. Fluid Mech.* **430**, 149–168.

Monkewitz, P. A., Chauhan, K. A. & Nagib, H. M. 2007 Self-consistent high-Reynolds-number asymptotics for zero-pressure-gradient turbulent boundary layers. *Phys. Fluids* **19** (115101).

Örlü, R. 2009 Experimental studies in jet flows and zero pressure-gradient turbulent boundary layers. PhD thesis, Department of Mechanics, KTH Stockholm, Sweden.

Örlü, R. & Alfredsson, P. H. 2010 On spatial resolution issues related to time-averaged quantities using hot-wire anemometry. *Exp. Fluids* **49**, 101–110.

Örlü, R., Fransson, J. H. M & Alfredsson, P. H. 2010 On near wall measurements of wall bounded flows–the necessity of an accurate determination of the wall position. *Prog. Aero. Sci.* **46**, 353–387.

Örlü, R. & Schlatter, P. 2011*a* On the fluctuating wall-shear stress in zero-pressure-gradient turbulent boundary layer flows. *Phys. Fluids* **23** (021704).

Örlü, R. & Schlatter, P. 2011*b* Turbulent boundary layers at moderate Reynolds numbers. Part II: Comparison simulation and experiment. Submitted.

Schlatter, P., Chevalier, M., Ilak, M. & Henningson, D. S. 2010*a* The structure of a turbulent boundary layer studied by numerical simulation. *arXiv* (1010.4000).

Schlatter, P., Li, Q., Brethouwer, G., Johansson, A. V. & Henningson, D. S. 2010*b* Simulations of spatially evolving turbulent boundary layers up to $Re_\theta = 4300$. *Int. J. Heat Fluid Flow* **31**, 251–261.

Schlatter, P., Li, Q., Brethouwer, G., Johansson, A. V. & Henningson, D. S. 2010*c* Structure of a turbulent boundary layer studied by DNS. In *Direct and Large-Eddy Simulation 8, July 7-9 2010*. To appear.

Schlatter, P. & Örlü, R. 2010*a* Assessment of direct numerical simulation data of turbulent boundary layers. *J. Fluid Mech.* **659**, 116–126.

Schlatter, P. & Örlü, R. 2010*b* Quantifying the interaction between large and small scales in wall-bounded turbulent flows: A note of caution. *Phys. Fluids* **22** (051704).

Schlatter, P. & Örlü, R. 2011 Turbulent boundary layers at moderate Reynolds numbers. Part I: Inflow length and tripping effects. Submitted.

Schlatter, P., Örlü, R., Li, Q., Brethouwer, G., Fransson, J. H. M., Johansson, A. V., Alfredsson, P. H. & Henningson, D. S. 2009 Turbulent boundary layers up to $Re_\theta = 2500$ studied through numerical simulation and experiments. *Phys. Fluids* **21** (051702).

Schlatter, P., Stolz, S. & Kleiser, L. 2004 LES of transitional flows using the approximate deconvolution model. *Int. J. Heat Fluid Flow* **25**, 549–558.

Segalini, A., Örlü, R., Schlatter, P., Alfredsson, P. H., Rüedi, J.-D. & Talamelli, A. 2011 A method to estimate turbulence intensity and transverse taylor microscale in turbulent flows from sptatially averaged hot-wire data. *Exp. Fluids* Online First.

Sharp, N. S., Neuscamman, S. & Warhaft, Z. 2009 Effects of large-scale free stream turbulence on a turbulent boundary layer. *Phys. Fluids* **21** (095105).

Simens, M. P., Jiménez, J., Hoyas, S. & Mizuno, Y. 2009 A high-resolution code for turbulent boundary layers. *J. Comput. Phys.* **228**, 4218–4231.

Simonich, J. C. & Bradshaw, P. 1978 Effect of free-stream turbulence on heat transfer through a turbulent boundary layer. *ASME J. Heat Transfer* **100**, 671–677.

Skote, M. 2001 Studies of turbulent boundary layer flow through direct numerical simulation. PhD thesis, Department of Mechanics, KTH Stockholm, Sweden.

Smits, A. J., Matheson, N. & Joubert, P. N. 1983 Low-Reynolds-number turbulent boundary layers in zero and favorable pressure gradients. *J. Ship Res.* **27**, 147–157.

Smits, A. J., McKeon, B. J. & Marusic, I. 2011 High Reynolds number wall turbulence. *Annu. Rev. Fluid Mech.* **43**, 353–375.

Spalart, P. R. 1988 Direct simulation of a turbulent boundary layer up to $R_\theta = 1410$. *J. Fluid Mech.* **187**, 61–98.

Talamelli, A., Persiani, F., Fransson, J. H. M., Alfredsson, P. H., Johansson, A. V., Nagib, H. M., Rüedi, J.-D., Sreenivasan, K. R. & Monkewitz, P. A. 2009 CICLoPE - a response to the need for high Reynolds number experiments. *Fluid Dyn. Res.* **41** (021407).

Wu, X. & Moin, P. 2008 A direct numerical simulation study on the mean velocity characteristics in turbulent pipe flow. *J. Fluid Mech.* **608**, 81–112.

Wu, X. & Moin, P. 2010 Transitional and turbulent boundary layer with heat transfer. *Phys. Fluids* **22**, 085105.